ACS APPLIED MATERIALS & INTERFACES

Research Article

www.acsami.org

Fully Converting Graphite into Graphene Oxide Hydrogels by Preoxidation with Impure Manganese Dioxide

Jiaojiao Sun, Ningxin Yang, Zhe Sun, Mengqi Zeng, Lei Fu, Chengguo Hu,* and Shengshui Hu

Key Laboratory of Analytical Chemistry for Biology and Medicine (Ministry of Education), College of Chemistry and Molecular Sciences, Wuhan University, Wuhan 430072, China

Supporting Information

ABSTRACT: Potassium permanganate ($KMnO_4$) has been proved to be an efficient oxidant for converting graphite into graphite oxide, but its slow diffusion in the interlayer of graphite seriously restricts the production of graphene oxide (GO). Here, we demonstrate that the preoxidation of graphite by impure manganese dioxide (MnO_2) in a mixture of concentrated sulfuric acid (H_2SO_4) and phosphorus pentoxide (P_2O_5) can efficiently improve the synthesis of GO when $KMnO_4$ is employed as the oxidant. The prepared honey-like GO hydrogels possess a high yield of single-layer sheets, large sizes (average lateral size up to 20 μm), wide ranges of stable dispersion concentrations (from dilute solutions, viscous hydrogels, to dry films), and good conductivity after reduction (~2.9 × 10^4 S/m). The mechanism for the improved synthesis of GO by impure MnO_2 was explored. The enhanced exfoliation and oxidation of graphite by oxidative Mn ions (mainly Mn^{3+}), which are synergistically produced by the reaction of impure MnO_2 with H_2SO_4 and P_2O_5, are found to be responsible for the improved synthesis of such GO hydrogels. Particularly, preoxidized graphite (POG) can be partially dispersed in water with sonication, which allows the facile construction of flexible and highly conductive graphene nanosheet film electrodes with excellent electrochemical sensing properties.

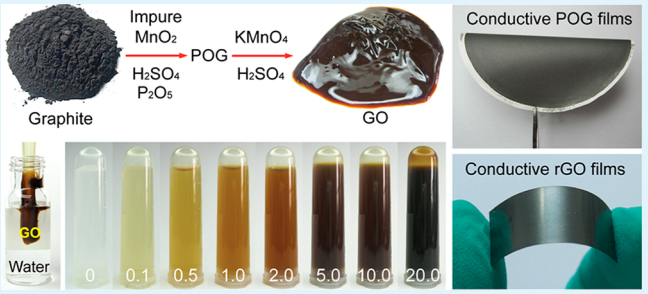

KEYWORDS: *graphene oxide, manganese dioxide, potassium permanganate, hydrogels, ion intercalated exfoliation*

1. INTRODUCTION

Graphene is currently a star material in material sciences because of its unique two-dimensional (2D) structure and intriguing physical and chemical properties for promising applications in a wide range of fields,[1,2] such as electronics,[3] electrochemistry,[4] sensors,[5,6] and so on. Although a variety of methods have been established for the synthesis of conductive graphene such as chemical vapor deposition (CVD),[7] mechanical exfoliation,[8] liquid sonication,[9] and electrochemical expansion,[10,11] a large proportion of the applications of graphene begin with graphene oxide (GO) considering its good processability, easy mass production from low-cost graphite, and good conductivity after reduction. Nowadays, the most widely used methods for the chemical synthesis of GO are the Hummers method[12] and several modified Hummers methods,[13,14] which use $KMnO_4$ as the main oxidant of graphite and some auxiliary agents for improving production yield of GO, including sodium nitrate ($NaNO_3$),[12] potassium persulfate ($K_2S_2O_8$),[13] and phosphoric acid (H_3PO_4).[14] Based on these works, some other strategies such as microwave heating,[8] multiple sonication,[15] optimizing oxidation conditions,[16,17] and post ionic intercalation[11] are also employed for the preparation of GO with large areas and high conductivity after reduction.

Contrary to extensive research on the synthesis method of GO, only a few works focus on its formation mechanism and structure evolution during synthesis.[18−20] For the chemical synthesis of GO from graphite, Kovtyukhova et al. found that the preoxidation of graphite by $K_2S_2O_8$ in concentrated H_2SO_4 was necessary for the production of GO when $KMnO_4$ was used as the main oxidant.[13] Otherwise, incompletely oxidized graphite-core/GO-shell particles were always observed in the final product. Tour et al. demonstrated that the formation of GO from graphite constituted three distinct independent steps, of which the diffusion of the oxidizing agent (e.g., $KMnO_4$) into the preoccupied graphite galleries of the sulfuric acid−graphite intercalation compound (H_2SO_4−GIC) was the rate-determining step of the entire process.[21] These works imply that the promoted diffusion of the oxidizing agent in the interlayer space of graphite should be an efficient approach to the improved synthesis of GO. This may be achieved either by increasing interlayer space via expansion[8,22] or by employing oxidants with small sizes and favorable charges.[10]

Here we demonstrate that the preoxidation of graphite by impure MnO_2 in the mixture of concentrated H_2SO_4 and P_2O_5 can efficiently improve the production yield of single-layer GO when $KMnO_4$ is employed as the oxidant. This method is able to produce honey-like GO hydrogels with excellent solution

Received: July 5, 2015
Accepted: September 9, 2015
Published: September 9, 2015

DOI: 10.1021/acsami.5b06008
ACS Appl. Mater. Interfaces 2015, 7, 21356−21363

dispersion and film formation ability but possessing good conductivity after reduction. The enhanced exfoliation and oxidation of graphite during preoxidation by oxidative and intercalative Mn ions (mainly Mn^{3+}), which are produced by the reaction of impure MnO_2 with concentrated H_2SO_4 and P_2O_5, are found to be responsible for the improved synthesis of such GO hydrogels. Moreover, our method provides two approaches to the construction of conductive graphene coatings from graphite for various applications: (1) a part of POG can be effectively exfoliated into water-dispersible and highly conductive graphene nanosheets by sonication, which is suitable for constructing flexible graphene film electrodes by vacuum filtration with excellent electrochemical sensing properties; (2) the as-prepared GO hydrogels, without any sonication or separation treatments, can be used for fabricating highly conductive and adhesive coatings on various substrates by using a modified hydroiodic acid (HI) reduction method. The present work thus not only proposes an efficient approach to the improved synthesis of GO but also demonstrates the promising applications of Mn^{3+} chemistry in carbon material sciences.

2. EXPERIMENTAL SECTION

2.1. Materials. Analytical reagent (AR) graphite was purchased from J&K Scientific Co., Ltd. (Beijing, China). Technically pure (T.P.) MnO_2 (~92%) was obtained from Adamas Reagent Co., Ltd. (Shanghai, China). Chemically pure (CP) MnO_2 (~72%) was purchased from Aladdin Reagent Co., Ltd. (Shanghai, China). AR Mn_2O_3 (99%) was purchased from Xiya Chemical Reagent Co., Ltd. (Chengdu, China). Potassium manganite (K_2MnO_4) was purchased from Alfa Aesar. Spectroscopically pure (SP) graphite, AR MnO_2 (99%), P_2O_5, $K_2S_2O_8$, $KMnO_4$, $NaNO_3$, H_2SO_4, potassium ferricyanide ($K_3Fe(CN)_6$), disodium hydrogen phosphate ($Na_2HPO_4 \cdot 12H_2O$), and sodium dihydrogen phosphate ($NaH_2PO_4 \cdot 2H_2O$) were purchased from Sinopharm Chemical Reagent Co., Ltd. (Shanghai, China). Dopamine was purchased from Acros. Potassium iodide (KI) was supplied by Kermel Chemical Reagent Co., Ltd. (Tianjin, China). Manganese(II) sulfate ($MnSO_4$) was obtained from Lingfeng Chemical Reagent Co., Ltd. (Shanghai, China). Phosphate buffer solutions (PBS, 0.1 M, pH 7.0) were prepared from $Na_2HPO_4 \cdot 12H_2O$ and $NaH_2PO_4 \cdot 2H_2O$ and adjusted to the desired pH value with 1.0 M HCl or NaOH by a pH meter (PB-10, Sartorius). Ultrapure deionized water (>18 MΩ·cm) was produced on Heal Force, Nison Instrument Ltd. (Shanghai, China).

2.2. Synthesis of Graphene Oxide. The procedures for the synthesis of GO by our method (GO_{TPMn}) were similar to Kovtyukhova's method[13] except for the replacement of $K_2S_2O_8$ by impure MnO_2 in the preoxidation step. Briefly, T.P. MnO_2 (2.0 g) and P_2O_5 (2.0 g) were gradually added to concentrated H_2SO_4 (10 mL) at 90 °C with stirring. After 10 min, the temperature was cooled to 80 °C and graphite (2.4 g) was slowly added. The mixture was allowed to react at 80 °C for 5 h, cooled to room temperature, carefully diluted with water (400 mL), and washed with water on a filter until the filtrate became neutral. The resulting POG was dried at 60 °C for 6 h and added to concentrated H_2SO_4 (92 mL) in an ice−water bath. Then $KMnO_4$ (12.0 g) was slowly added with stirring to control the temperature below 5 °C. The mixture was stirred at 35 °C for 2 h, diluted with ice−water (200 mL) and heated to 48 °C for 2 h. Afterward, the mixture was cooled to room temperature and diluted with water (600 mL). Then 30% H_2O_2 (10 mL) was added dropwise with strong stirring. The brown sediment was washed by HCl (10 wt %) for at least six times to remove trace metal ions, each for 0.5 h. The mixture was allowed to stand overnight, washed with copious water, and dialyzed in water for at least 5 days, producing a honey-like GO hydrogel.

The procedures for the synthesis of GO by AR MnO_2, CP MnO_2, AR Mn_2O_3, or their mixtures were similar to those of GO_{TPMn} by using the same or varied mass ratios of the corresponding manganese oxides. For the synthesis of GO using $NaNO_3$ (GO_N) or $K_2S_2O_8$ (GO_S) as the auxiliary agent, they were prepared according to previous works.[12,13]

2.3. Fabrication of rGO Films. GO films on polyethylene terephthalate (PET) were fabricated by screen printing GO solutions (~33 mg/mL) on a PET substrate, followed by drying at 60 °C for 5 h. The resulting GO-PET composite film was reduced in a mixture of HCl and KI at a concentration of 25 mg/mL KI in concentrated HCl for 35 min at room temperature. During this process, the color of the GO film turned from brown to black. Subsequently, the film was thoroughly rinsed with water and dried at 60 °C for 5 h.

2.4. Characterizations. Scanning electron microscope (SEM) images were collected on a Zeiss sigma field emission SEM system. Transmission electron microscope (TEM) tests were performed using JEM-2100 (HR). The thickness of GO was tested on a NT-MDT NTEGRA Spectra atomic force microscope (AFM) under a semicontact mode. X-ray diffraction (XRD) measurements were taken on a Bruker D8 Discover equipped with Cu Kα irradiation (k = 1.5406 Å). Raman spectra were obtained using a Renishaw Raman RM-1000 at an excitation wavelength of 514.5 nm. XPS spectra were collected on Kratos Analytical XSAM 800, UV−vis spectra were performed on a UV 2550 UV−vis spectrophotometer, and FTIR spectra were obtained on a Magna-IR 550 spectrometer. Optical microscope images were collected on a digital microscope (XSP-8CA). Sheet resistance of rGO films was measured with a four-point probe sheet resistance tester (ST-21H, China). Kinematic viscosity of GO_{TPMn} solutions was tested using a Ubbelohde viscometer with an inner diameter of 0.7−0.8 mm and a viscometer constant of 0.0294 mm^2/s^2 at 20 °C.

3. RESULTS AND DISCUSSION

3.1. Solution Dispersion and Film Formation Ability of GO. Our method is established on the basis of a two-step process similar to the widely used modified Hummers method proposed by Kovtyukhova et al.[13] except for the employment of impure MnO_2 in the preoxidation step (Figure 1a). Our

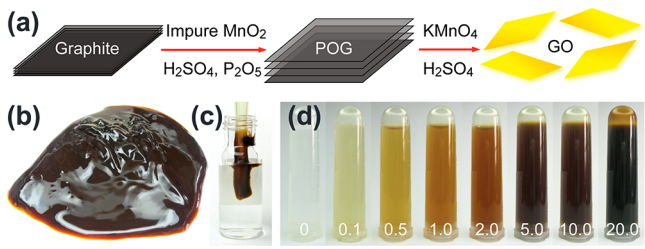

Figure 1. (a) Schematic procedures for the synthesis of GO_{TPMn} by our method. (b) As-dialyzed GO_{TPMn} hydrogels on glass. (c) GO_{TPMn} hydrogels in water. (d) Aqueous solutions of GO_{TPMn} with varied concentrations at mg/mL levels.

DOI: 10.1021/acsami.5b06008
ACS Appl. Mater. Interfaces 2015, 7, 21356−21363

method is able to produce a honey-like GO hydrogel from SP graphite using T.P. MnO_2 as the preoxidant (GO_{TPMn}) at a production yield of about 100% after dialysis and without sonication (Figure 1b and 1c). Here a gel is defined as a non-fluid colloidal or polymer network expanded throughout its whole volume by a fluid. If the swelling agent is water and the network component is GO or its composites, it is referred to as a GO hydrogel.[23,24] The GO_{TPMn} hydrogel is readily dispersible in water in a wide concentration range by simply shaking the mixture of the GO_{TPMn} hydrogel and water (Figure 1d), of which the stability can be further improved through a very short period of sonication (e.g., 1 min) (Figure S1, Supporting Information). GO_{TPMn} possesses apparently better solution dispersion ability and film formation quality compared with the GO prepared from the same SP graphite using $K_2S_2O_8$[13] as the preoxidant (denoted as GO_S) (Figures S2 and S3, Supporting Information), which was proved to be mainly due to the apparently improved yield of single-layer GO by T.P. MnO_2 (Figure S4, Supporting Information). GO_{TPMn} will spontaneously assemble into highly compact and smooth films during drying (Figure S5, Supporting Information), which could be hardly converted into powder even with strong grinding. The resulting dry GO_{TPMn} films are redispersible in water with the aid of sonication or agitation, producing stable aqueous dispersions at low concentrations or viscous hydrogels at concentrations higher than 2.5 wt % (Figure S6, Supporting Information).

According to Shi et al.,[23,24] the formation of GO hydrogels can be achieved by different driving forces such as hydrogen bonding, electrostatic interaction, coordination, and $\pi-\pi$ interactions with the aid of additional additives at relatively low concentrations. In our case, the formation of GO_{TPMn} hydrogels at relatively high concentrations in pure water should mainly arise from the π-stacking and hydrophobic interactions between adjacent GO sheets because (1) the absence of additional additives excludes the formation of GO hydrogels by electrostatic and coordination interactions, and (2) the higher oxidation extent of GO_{TPMn} led to less gelation extent (Figure S7, Supporting Information), which excludes the dominant role of hydrogen bonding for hydrogel formation. This assumption is also supported by the destruction of a 40 mg/mL GO_{TPMn} hydrogel with ethanol and the re-gelation of the solution by ferrocene (Fc) (Figure S8, Supporting Information). In fact, the critical roles of π-stacking and hydrophobic interactions in the formation of GO hydrogels with or without additives such as Fc have been reported in several previous works.[23,25,26] The GO_{TPMn} hydrogel prepared from SP graphite has a critical gel concentration (CGC) of about 25 mg/mL. Below this CGC, the GO_{TPMn} aqueous solution becomes more viscous with increasing the solution concentration, and the kinematic viscosities of 0, 5.0, and 10.0 mg/mL GO_{TPMn} solutions determined with a Ubbelohde viscometer are 1.000, 1.444, and 6.327 mm^2/s, respectively. With the increase of GO_{TPMn} concentration above the CGC, the viscosity of the paste-like GO_{TPMn} hydrogel is continuously enhanced until the formation of dry films or blocks (Figures S5 and S6, Supporting Information).

3.2. Structure and Conductivity Characterizations of GO. The structural properties between GO_{TPMn} and GO prepared by several widely used Hummers methods[12,13] are compared (Figure 2). Obviously, no significant differences between GO_{TPMn} and other GO products are observed on FTIR (Figure 2a), Raman (Figure 2b) and C 1s X-ray photoelectron (XPS) spectra (Figure 2c) except for the variation in mass ratio of different functionalities (Figure S9, Supporting Information). Moreover, the carbon-to-oxygen ratios (C/O) are 3.17, 2.70, and 2.47 for GO prepared by the original Hummers method (GO_N), GO_S, and GO_{TPMn}, respectively (Figure S10, Supporting Information). These results reveal a very similar structure but a slightly higher oxidation extent of GO_{TPMn} compared with GO prepared by other Hummers methods.[12,13] The conductivity of reduced GO (rGO) films prepared from different GO by a modified HI method[27] was also examined (Figure 2d and Supporting Information). The conductivity of the rGO film prepared from GO_{TPMn} without sonication is close to that of sonicated GO_s and GO_N. However, the sonication treatment apparently increases the sheet resistance of GO_{TPMn}. As indicated by Figures S4c and S11, the sonication treatment led to the apparent destruction of GO sheets into smaller fragments. Therefore, the decreased conductivity of the rGO film for the sonicated GO_{TPMn} should arise from the decline of GO sheet size.[28]

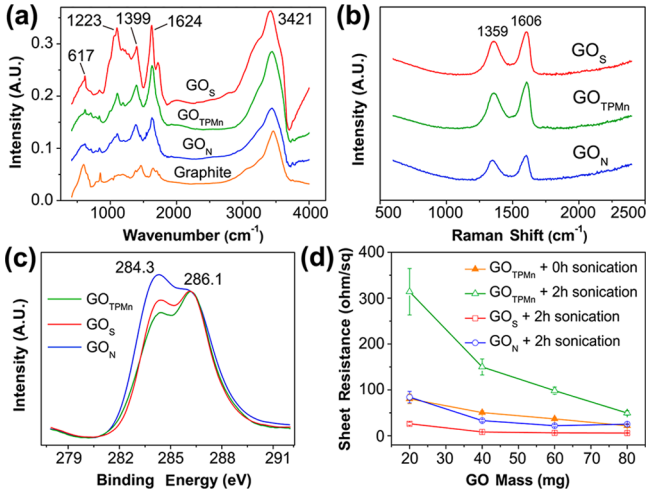

Figure 2. Spectroscopic characterizations of GO prepared from SP graphite with different Hummers methods by FTIR (a), Raman (b), and XPS spectra (c). (d) Dependence of sheet resistance on the surface loading of the rGO films. All the XPS spectra were normalized at the peak position of 286.1 eV.

3.3. Enhanced Exfoliation of Graphite by Preoxidation with Impure MnO_2. On the basis of the above discussions, it is obvious that GO_{TPMn} has a structure similar to GO_S but possesses a higher production yield of single-layer GO. Further investigations demonstrated that the employment of MnO_2 with higher purity (e.g., AR MnO_2) as the preoxidant conversely led to the quality decline of GO (denoted as GO_{ARMn}) (Figure S12a, Supporting Information). To understand the mechanism for the improved synthesis of GO_{TPMn}, we monitored the morphologic change of graphite during synthesis. The results indicated that no apparent difference appeared during the preoxidation process of graphite by $K_2S_2O_8$, AR MnO_2, and T.P. MnO_2 (not shown). However, significant differences were observed during the further oxidation of POG by $KMnO_4$ (Figure 3), i.e., POG prepared with T.P. MnO_2 (denoted as POG_{TPMn}) is more rapidly converted into nanosheets as compared with POG prepared with either AR MnO_2 (denoted as POG_{ARMn}) or $K_2S_2O_8$ (denoted as POG_S). Particularly, POG_S is slowly decomposed into semitransparent granular crystals after 2 h oxidation with

DOI: 10.1021/acsami.5b06008
ACS Appl. Mater. Interfaces 2015, 7, 21356−21363

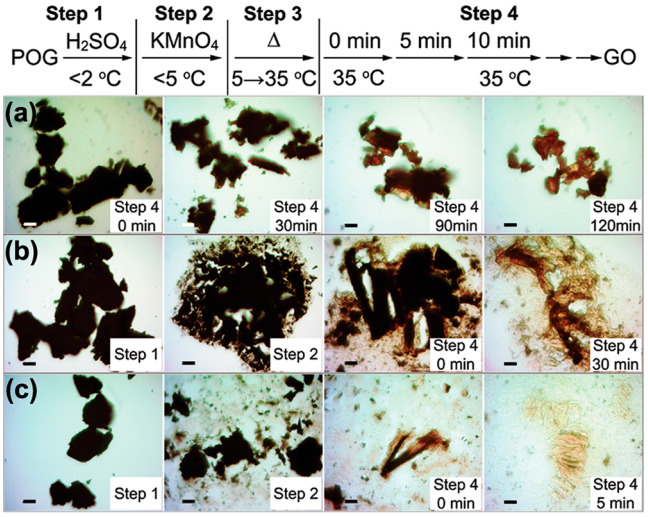

Figure 3. Optical microscope images on the evolution of shape, size, and color of POG during the oxidation process to graphite oxide by $KMnO_4$: (a) POG_S; (b) POG_{ARMn}; (c) POG_{TPMn}. Scale bars are 20 μm.

$KMnO_4$, whereas no granular particles are observed for POG_{TPMn} after only 5 min oxidation by $KMnO_4$ at 35 °C. These results clearly imply the much higher exfoliation efficiency of graphite by preoxidation with T.P. MnO_2.

We examined the structural property of POG_{TPMn}, POG_S, and graphite by FTIR, XPS, and XRD spectra (Figure 4). The

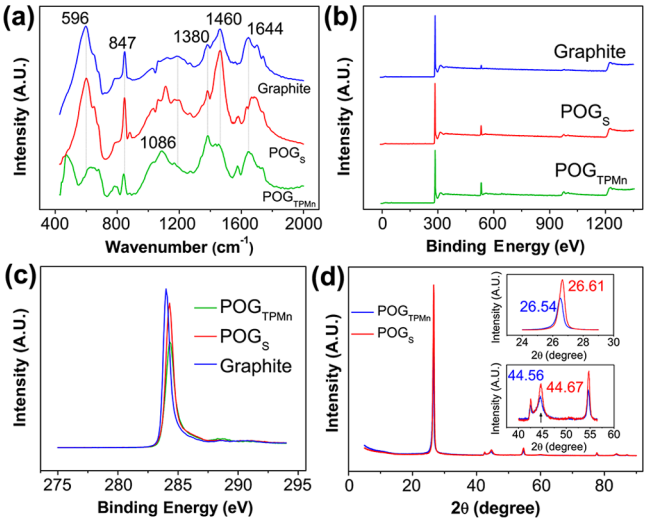

Figure 4. Spectroscopic characterizations of POG_{TPMn}, POG_S, and graphite by FTIR (a), XPS (b, c), and XRD spectra (d). Insets of part d are the amplified plots of the corresponding regions on the XRD spectra.

FTIR spectrum of POG_S is in between those of POG_{TPMn} and graphite (Figure 4a), and the structure difference between POG_{TPMn} and graphite is smaller than that between GO_{TPMn} and graphite (Figure S13, Supporting Information). This result suggests the partial preservation of the structure of graphite after preoxidation by impure MnO_2. Furthermore, the C/O ratios are 30.75, 7.44, and 12.21 for graphite, POG_{TPMn}, and POG_S, respectively (Figure 4b), revealing a low amount of oxygen-related groups on these POG (Figure 4c). Therefore, although the oxidation extent of POG_{TPMn} is higher than that of POG_S, the large π-structure of graphite is not seriously destroyed during preoxidation by either T.P. MnO_2 or $K_2S_2O_8$, which is supported by the good conductivity of the POG powders (Figure S14, Supporting Information). In addition, all the peaks in the XRD spectra of POG_{TPMn} slightly shift to the negative direction as compared with those of POG_S (Figure 4d and Table S1), which is indicative of better exfoliation.[29] Actually, a part of POG_{TPMn} can be dispersed in water with good stability by sonication, whereas most of POG_S sediments within 5 min (Figure S15, Supporting Information). Therefore, the large difference between GO_{TPMn} and GO_S should mainly arise from the different oxidation and exfoliation extent of POG_{TPMn} and POG_S. As indicated above, the C/O ratio of POG_{TPMn} is apparently lower than that of POG_S, which seems to collide with the oxidation capacity of MnO_2 and $K_2S_2O_8$, i.e., the standard reduction potential (E°) of $K_2S_2O_8$ ($S_2O_8^{2-} + 2H^+ + 2e^- = 2HSO_4^-$, + 2.12 V) is apparently higher than that of MnO_2 ($MnO_2 + 4H^+ + 2e^- = Mn^{2+} + 2H_2O$, +1.22 V) in acidic media.[30] These results imply that the different performance of impure MnO_2 and $K_2S_2O_8$ on the synthesis of GO should be mainly due to their difference in parameters such as sizes or charges instead of redox potentials.

3.4. Identification of Mn^{3+} for Improved Synthesis of GO by Impure MnO_2. To find the origin of the active impurities in T.P. MnO_2, we investigated the variation of the color and UV−vis spectra with reaction period for a reaction mixture of H_2SO_4, P_2O_5, and different Mn compounds (Figure 5). In the case of AR MnO_2, the color of the reaction mixture

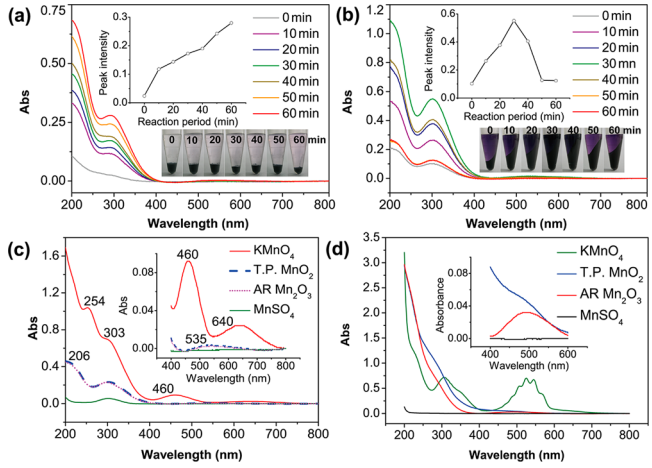

Figure 5. (a, b) Dependence of UV−vis spectra on the reaction period of AR MnO_2 (a) and T.P. MnO_2 (b) in a mixture of concentrated H_2SO_4 and P_2O_5. (c, d) UV−vis spectra of $KMnO_4$, T.P. MnO_2, AR Mn_2O_3, and $MnSO_4$ in concentrated (c) and dilute H_2SO_4 (d). Insets of a and b are the photos of the reaction mixtures at different reaction periods. Insets of c and d illustrate the amplified spectra in the range of 400−800 nm. Prior to UV−vis measurements, the sample solutions of AR MnO_2 and T.P. MnO_2 for parts a and b were diluted with concentrated H_2SO_4 3- and 60-fold, respectively. Detailed information for preparing the sample solutions is provided in Supporting Information.

gradually changes from colorless to very light purple by increasing reaction time (Figure 5a). Accompanied by this, two UV−vis absorption peaks appear and gradually increase, suggesting the production of new species during reaction. In contrast, the purple color of the reaction mixture of T.P. MnO_2 is much stronger than that of AR MnO_2 at the very beginning,

DOI: 10.1021/acsami.5b06008
ACS Appl. Mater. Interfaces 2015, 7, 21356−21363

which is first enhanced and then weakened after a reaction period of 30 min (Figure 5b). This phenomenon is well consistent with the variation of the UV−vis spectra. Considering the improved synthesis of GO by T.P. MnO_2 as compared with AR MnO_2, it is convincible that the purple active species produced in the reaction mixture of H_2SO_4, P_2O_5, and T.P. MnO_2 should be responsible for the successful synthesis of the honey-like GO_{TPMn}. Actually, the isolated purple solution of the mixture of T.P. MnO_2, concentrated H_2SO_4, and P_2O_5 also effectively improved the synthesis of GO.

Figure 5c shows the UV−vis spectra of different Mn compounds in concentrated H_2SO_4. It is clear that the UV−vis spectrum of T.P. MnO_2 is different from that of $KMnO_4$ and $MnSO_4$, reflected by the appearance of the absorptions at 254, 303, 460, and 640 nm for $KMnO_4$, the peaks at 206, 303, and 535 nm for T.P. MnO_2 and the peak at 303 nm for $MnSO_4$. Meanwhile, the UV−vis spectrum of T.P. MnO_2 is nearly overlapped with that of AR Mn_2O_3. A similar relationship between the UV−vis spectra of these species in dilute H_2SO_4 is also observed (Figure 5d). In fact, the different existing forms of these Mn compounds in concentrated H_2SO_4 can be directly observed by the naked eye, i.e., the colors for the solutions of $KMnO_4$, T.P. MnO_2 and $MnSO_4$ in concentrated H_2SO_4 are blackish green, purple, and colorless, respectively. Therefore, the purple active species should not come from MnO_4^- or Mn^{2+} but is likely due to manganese(III) ion (Mn^{3+}). Here the role of manganese(IV) ions (Mn^{4+}) in the synthesis of GO_{TPMn} may be less important considering the following facts: (1) the concentration of the purple species for AR MnO_2 in concentrated H_2SO_4 is much lower than that of T.P. MnO_2 (Figure 5a and 5b); (2) the UV−vis spectrum of T.P. MnO_2 in H_2SO_4 is almost overlapped with that of AR Mn_2O_3 (Figure 5c); (3) the quality of GO prepared by AR Mn_2O_3 was found to be better than that of AR MnO_2 (Figure S12a, Supporting Information).

Selim and Lingane demonstrated that the formal disproportionation constant for the reaction of $2Mn^{3+} = Mn^{4+} + Mn^{2+}$ varied from 10^{-3} in 4 M sulfuric acid to 10^{-4} in 7 M H_2SO_4 at 25°, which suggests the much higher stability of Mn^{3+} in concentrated H_2SO_4 compared with Mn^{4+}.[31] Moreover, for the reaction system of oxidizing Mn^{2+} with MnO_4^- in acidic media, Cheney[32] and Gosh[33] concluded that the reaction between Mn(VII) and Mn(II) occurs stoichiometrically to yield Mn(III) in acidic medium, and Mn(III) produced in this reaction is stable for months in highly acidic medium, such as in 4.5 M aqueous sulfuric acid.[32] These works indicate that the contemporary use of concentrated H_2SO_4 and P_2O_5 here should similarly ensure the existence of Mn^{3+} with relatively high concentrations in the reaction medium by complexation or ion pair interactions,[21] which may be responsible for the enhanced exfoliation of POG_{TPMn}.

3.5. Mechanism for Improved Synthesis of GO by Impure MnO_2. To further verify the role of Mn^{3+}, we prepared a simulated sample of T.P. MnO_2 by mixing AR Mn_2O_3 with AR MnO_2 at a mass ratio of 8:92 and grinding the mixture for 1 h with a ball milling machine, which was then used as the preoxidant for the synthesis of GO. The result indicated that the quality of GO prepared in this manner was even better than that of GO_{TPMn} (Figure S12b, Supporting Information). However, when one part of the above mixture, i.e., 8 wt % AR Mn_2O_3 alone, was used as the preoxidant, the quality of the synthesized GO was rather poor (Figure S12b, Supporting Information). Therefore, although Mn^{3+} should be the main active species for the synthesis of GO_{TPMn}, Mn(IV) in impure MnO_2 may also contribute to this process, probably through the reaction with Mn^{2+} to regenerate Mn^{3+} (Figure S16, Supporting Information).[34] We further examined the oxidation states of Mn in impure MnO_2 by Mn 2p XPS spectra (Figure 6). The results indicate that the Mn $2p_{3/2}$ and Mn $2p_{1/2}$ peaks

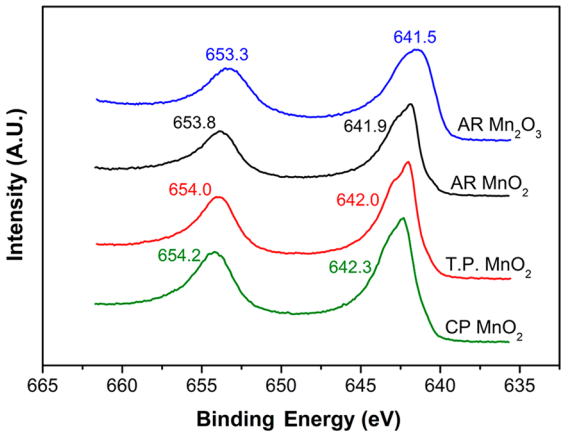

Figure 6. Mn 2p XPS spectra of AR Mn_2O_3, AR MnO_2, T.P. MnO_2, and CP MnO_2.

of T.P. and CP MnO_2 apparently shift to the positive direction compared with those of AR MnO_2 and AR Mn_2O_3, revealing the presence of Mn oxide impurities with oxidation states higher than Mn(IV) in impure MnO_2.[35] This conclusion seems to collide with the essential role of Mn^{3+} in the synthesis of GO_{TPMn} because of the absence of Mn(III) in impure MnO_2. However, it should be pointed out that Mn oxides with oxidation states higher than Mn(IV) (e.g., Mn(VI)) may be unstable in acidic media as in the case of K_2MnO_4 (Figure S17, Supporting Information), leading to the formation of Mn^{3+} by the reaction of impure MnO_2 with concentrated H_2SO_4 and P_2O_5 (see Figure 5b).

For the chemical synthesis of GO by oxidizing graphite in concentrated H_2SO_4 with $KMnO_4$, Tour et al. found that graphite is first intercalated by H_2SO_4 within 3−5 min, producing a H_2SO_4−GIC compound with H_2SO_4 molecules and HSO_4^- ions packing into the interlayer galleries.[21] Similarly, for the preoxidation of graphite by $K_2S_2O_8$ or impure MnO_2 in the mixture of H_2SO_4 and P_2O_5, the reaction should be initiated by the formation of the H_2SO_4−GIC compound and followed by the diffusion of the oxidizing agent, i.e., $S_2O_8^{2-}$ or Mn^{3+}, in the interlayer of H_2SO_4−GIC. In this context, Mn^{3+} may more rapidly diffuse into the interlayer of H_2SO_4−GIC than $S_2O_8^{2-}$ by a possible ion exchange mechanism and its small size.[36] Similar enhanced intercalation and exfoliation of graphite by small-sized surfactants[37] and organic solvents[38] have been employed for the synthesis of graphene by simple sonication methods. In addition, ion intercalation[39] has been successfully employed for the efficient exfoliation of graphite to prepare few-layer graphene by electrochemical methods using Li^+[10] or tetraalkylammonium cations[40] as the intercalation agent. Therefore, the suitable oxidation capacity, small size, positive charges, and relatively high concentration of Mn^{3+} in a mixture of concentrated H_2SO_4 and P_2O_5, together with its regeneration by the reaction between MnO_2 and Mn^{2+}, enable the efficient exfoliation and oxidation of graphite by

DOI: 10.1021/acsami.5b06008
ACS Appl. Mater. Interfaces 2015, 7, 21356−21363

preoxidation with impure MnO_2 for the improved synthesis of GO by $KMnO_4$ (Scheme 1).

Scheme 1. Schematic Representation for the Enhanced Exfoliation and Oxidation of Graphite by Mn^{3+} Ions That Are Synergistically Produced in the Reaction of Impure MnO_2 with H_2SO_4 and P_2O_5[a]

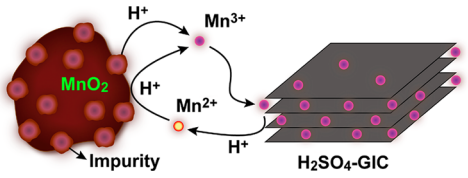

[a]The possible coordination interactions between anions (e.g., SO_4^{2-}) and Mn^{3+} are omitted to simplify the illustration.

3.6. Potential Applications. Lateral size has great influence on the application performance of graphene in fields such as three-dimensional graphene-based networks and optoelectronic devices.[15] For instance, the enlargement of GO size can decrease the number of intersheet tunneling barriers in a continuous rGO film and apparently improves the conductivity, which is essential to the practical applications of rGO-based transparent conductive films (TCFs) in flat displays, solar cells, optical communication devices, and solid-state lighting.[16] Similarly, the lateral dimension of GO sheets is a key factor for deciding their gelating ability, and the larger size of GO generally leads to a relatively lower CGC.[24] Here the employment of AR graphite flakes (purity >99%, J&K Chemicals, China) enables the synthesis of GO sheets with large sizes. Similar to the case of SP graphite, the preoxdation of graphite with impure MnO_2 can produce GO with better solution dispersion ability and exfoliation efficiency compared with the case of $K_2S_2O_8$ (Figure 7a–c). Clearly, GO_{TPMn} prepared from the AR graphite possesses large sizes (average lateral sizes >20 μm) and a high production yield of single-layer sheets (Figure S18, Supporting Information). The height of single-layer GO_{TPMn} produced by our method is about 1.1 nm by atomic force microscope (AFM) measurements (Figure 7d),

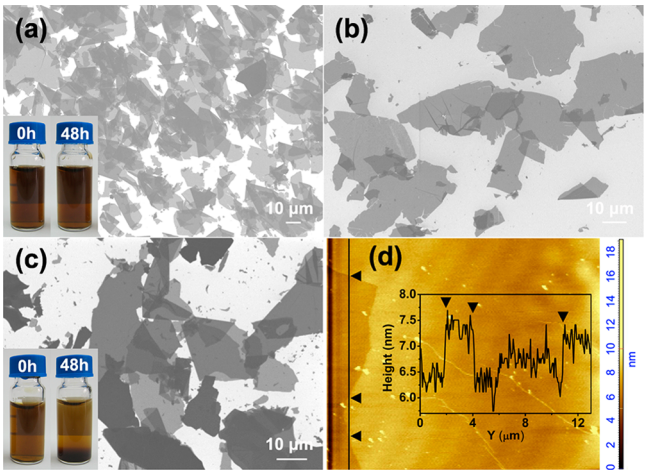

Figure 7. SEM (a–c) and AFM images (d) of GO_{TPMn} (a, b, d) and GO_S (c) prepared from AR graphite. Insets of a and c are the photos of the aqueous solutions of GO_{TPMn} and GO_S with different sedimentation periods after 1 min sonication. Inset of d shows the height profile of a large GO_{TPMn} sheet.

which is consistent with the height of single-layer GO sheets reported previously.[14,16]

The as-prepared GO_{TPMn} hydrogels can be directly used for the screen printing of smooth, ultrathin, and tightly bound GO coatings on various substrates such as PET (Figure 8a), which

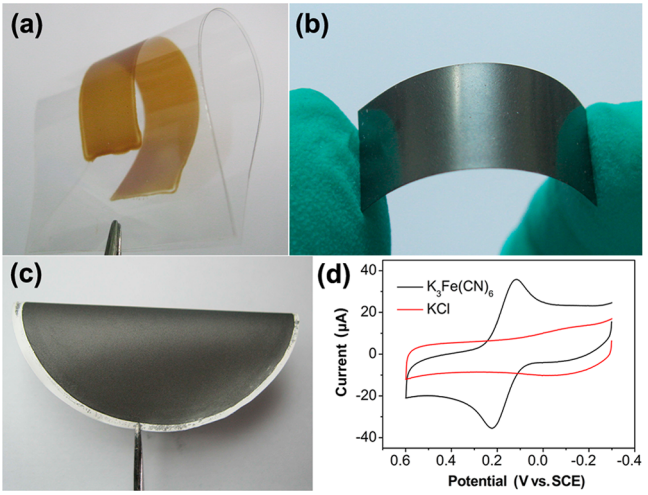

Figure 8. (a, b) Photos of a screen-printed GO film on PET (a) and its rGO film reduced by the modified HI method (b). (c) Photo of a graphene nanosheet film on a cellulose filtering membrane prepared from POG_{TPMn} by sonication and vacuum filtration. (d) Cyclic voltammograms of a graphene nanosheet film electrode prepared from c in 0.1 M KCl with and without 5.0 mM $K_3Fe(CN)_6$ at a scan rate 100 mV/s. The starting material for a–d was SP graphite.

is readily converted into highly conductive and strongly adhesive rGO coatings by simply placing the composite in the mixture solution of KI and HCl for a certain period (Figure 8b, and Figures S19 and S20, Supporting Information). The conductivity of the rGO film prepared in this manner is about 1.2×10^4 and 2.9×10^4 S/m using SP graphite and AR graphite as the starting material, respectively. Comparing Figure S4a with Figure 7b, it is clear that the conductivity of the rGO film is directly related to the size of GO sheets, i.e., the larger lateral size of GO generally produces rGO films with higher conductivity. Moreover, the kinematic viscosity of 5.0 mg/mL GO_{TPMn} in water is changed from 1.444 to 13.233 mm^2/s when the starting material is changed from SP graphite to AR graphite, which suggests the enhanced viscosity of the GO_{TPMn} solution with larger lateral sizes. As indicated by Figures S14 and S15, our method is also able to produce POG with good conductivity and exfoliation efficiency, thus providing a chance for the preparation of water dispersible and highly conductive graphene nanosheets with thickness of tens of nanometers and size of several micrometers by simply sonicating POG_{TPMn} in water for a certain period (e.g., 1 h) (Figure S21, Supporting Information). The partial dispersion of POG_{TPMn} in water should arise from its efficient exfoliation into nanosheets and the introduction of hydrophilic oxygen-related groups during preoxidation (Figures 4 and S22). This graphene nanosheet solution can form compact, smooth, and highly conductive films by vacuum filtration, which possess a low sheet resistance of ~40 ohm/sqr for 20 mg graphene nanosheets on a cellulose filtering membranes of 50 mm in diameter (Figure 8c). The resulting flexible graphene film electrode (Figure S23, Supporting Information) exhibits excellent responses toward typical electrochemical probes such as $K_3Fe(CN)_6$ (Figure 8d)

DOI: 10.1021/acsami.5b06008
ACS Appl. Mater. Interfaces 2015, 7, 21356–21363

and dopamine (Figure S24, Supporting Information), resembling the electrochemical behaviors of carbon nanotube-modified electrodes[41] and demonstrating its promising applications in the field of electrochemical sensing. In contrast, the rGO film electrode prepared from either AR or SP graphite by the modified HI method possessed rather poor electrochemical activity (Figure S25, Supporting Information).

4. CONCLUSIONS

In summary, we demonstrate here that the preoxidation of graphite by impure MnO_2 in the mixture of concentrated H_2SO_4 and P_2O_5 is able to fully convert graphite from different sources into honey-like GO hydrogels when $KMnO_4$ is employed as the oxidant. The established new modified Hummers method has several advantages for the synthesis of GO, including high yield of single-layer GO sheets, wide ranges of stable dispersion concentrations, excellent film formation ability, and good conductivity after reduction. Moreover, the preoxidized graphite can be partially dispersed in water by sonication, producing a highly conductive graphene nanosheet solution that allows the facile construction of flexible graphene film electrodes with good electrochemical sensing performance. The mechanism for the improved synthesis of GO by impure MnO_2 was explored. Oxidative Mn^{3+} ions, which are produced by the synergistic reaction of impure MnO_2 with a mixture of concentrated H_2SO_4 and P_2O_5, were found to be responsible for the enhanced exfoliation and oxidation of graphite and the successful synthesis of the honey-like GO_{TPMn}.

■ ASSOCIATED CONTENT

Supporting Information

The Supporting Information is available free of charge on the ACS Publications website at DOI: 10.1021/acsami.5b06008.

Procedures for preparing test samples of conductivity and UV−vis spectra; photos for solution dispersion and film formation ability of GO and rGO; XRD, XPS, FTIR, and UV−vis data of GO and POG; SEM images of GO and rGO films; CV responses of rGO and POG films (PDF)

■ AUTHOR INFORMATION

Corresponding Author

*Fax: +86-27-68754067. E-mail: cghu@whu.edu.cn.

Notes

The authors declare no competing financial interest.

■ ACKNOWLEDGMENTS

We appreciate the financial support from the National Nature Science Foundation of China (no. 20805035), the Fundamental Research Funds for the Central Universities (no. 2042014kf0244), the Natural Science Foundation of Hubei Province (no. 2015CFB538), and the Large-scale Instrument and Equipment Sharing Foundation of Wuhan University.

■ REFERENCES

(1) Allen, M. J.; Tung, V. C.; Kaner, R. B. Honeycomb Carbon: A Review of Graphene. *Chem. Rev.* **2010**, *110*, 132−145.
(2) Zhu, Y. W.; Murali, S.; Cai, W. W.; Li, X. S.; Suk, J. W.; Potts, J. R.; Ruoff, R. S. Graphene and Graphene Oxide: Synthesis, Properties, and Applications. *Adv. Mater.* **2010**, *22*, 3906−3924.
(3) Wu, J.; Pisula, W.; Müllen, K. Graphenes as Potential Material for Electronics. *Chem. Rev.* **2007**, *107*, 718−747.
(4) Ambrosi, A.; Chua, C. K.; Bonanni, A.; Pumera, M. Electrochemistry of Graphene and Related Materials. *Chem. Rev.* **2014**, *114*, 7150−7188.
(5) Chen, D.; Feng, H.; Li, J. Graphene Oxide: Preparation, Functionalization, and Electrochemical Applications. *Chem. Rev.* **2012**, *112*, 6027−6053.
(6) Wu, S.; He, Q.; Tan, C.; Wang, Y.; Zhang, H. Graphene-Based Electrochemical Sensors. *Small* **2013**, *9*, 1160−1172.
(7) Qiu, L.; Liu, J. Z.; Chang, S. L. Y.; Wu, Y.; Li, D. Biomimetic Superelastic Graphene-Based Cellular Monoliths. *Nat. Commun.* **2012**, *3*, 1241.
(8) Luo, Z.; Lu, Y.; Somers, L. A.; Johnson, A. T. C. High Yield Preparation of Macroscopic Graphene Oxide Membranes. *J. Am. Chem. Soc.* **2009**, *131*, 898−899.
(9) Coleman, J. N. Liquid Exfoliation of Defect-Free Graphene. *Acc. Chem. Res.* **2013**, *46*, 14−22.
(10) Wang, J.; Manga, K. K.; Bao, Q.; Loh, K. P. High-Yield Synthesis of Few-Layer Graphene Flakes through Electrochemical Expansion of Graphite in Propylene Carbonate Electrolyte. *J. Am. Chem. Soc.* **2011**, *133*, 8888−8891.
(11) Ang, P. K.; Wang, S.; Bao, Q.; Thong, J. T. L.; Loh, K. P. High-Throughput Synthesis of Graphene by Intercalation−Exfoliation of Graphite Oxide and Study of Ionic Screening in Graphene Transistor. *ACS Nano* **2009**, *3*, 3587−3594.
(12) Hummers, W. S.; Offeman, R. E. Preparation of Graphitic Oxide. *J. Am. Chem. Soc.* **1958**, *80*, 1339−1339.
(13) Kovtyukhova, N. I.; Ollivier, P. J.; Martin, B. R.; Mallouk, T. E.; Chizhik, S. A.; Buzaneva, E. V.; Gorchinskiy, A. D. Layer-by-Layer Assembly of Ultrathin Composite Films from Micron-Sized Graphite Oxide Sheets and Polycations. *Chem. Mater.* **1999**, *11*, 771−778.
(14) Marcano, D. C.; Kosynkin, D. V.; Berlin, J. M.; Sinitskii, A.; Sun, Z.; Slesarev, A.; Alemany, L. B.; Lu, W.; Tour, J. M. Improved Synthesis of Graphene Oxide. *ACS Nano* **2010**, *4*, 4806−4814.
(15) Sierra, U.; Álvarez, P.; Santamaría, R.; Granda, M.; Blanco, C.; Menéndez, R. A Multi-step Exfoliation Approach to Maintain the Lateral Size of Graphene Oxide Sheets. *Carbon* **2014**, *80*, 830−832.
(16) Zhao, J.; Pei, S.; Ren, W.; Gao, L.; Cheng, H.-M. Efficient Preparation of Large-Area Graphene Oxide Sheets for Transparent Conductive Films. *ACS Nano* **2010**, *4*, 5245−5252.
(17) Eigler, S.; Enzelberger-Heim, M.; Grimm, S.; Hofmann, P.; Kroener, W.; Geworski, A.; Dotzer, C.; Röckert, M.; Xiao, J.; Papp, C.; Lytken, O.; Steinrück, H.-P.; Müller, P.; Hirsch, A. Wet Chemical Synthesis of Graphene. *Adv. Mater.* **2013**, *25*, 3583−3587.
(18) Dreyer, D. R.; Park, S.; Bielawski, C. W.; Ruoff, R. S. The Chemistry of Graphene Oxide. *Chem. Soc. Rev.* **2010**, *39*, 228−240.
(19) Yang, J.; Shi, G.; Tu, Y.; Fang, H. High Correlation between Oxidation Loci on Graphene Oxide. *Angew. Chem., Int. Ed.* **2014**, *53*, 10190−10194.
(20) Yang, L.; Zhang, R.; Liu, B.; Wang, J.; Wang, S.; Han, M.-Y.; Zhang, Z. π-Conjugated Carbon Radicals at Graphene Oxide to Initiate Ultrastrong Chemiluminescence. *Angew. Chem., Int. Ed.* **2014**, *53*, 10109−10113.
(21) Dimiev, A. M.; Tour, J. M. Mechanism of Graphene Oxide Formation. *ACS Nano* **2014**, *8*, 3060−3068.
(22) Hong, Y.; Wang, Z.; Jin, X. Sulfuric Acid Intercalated Graphite Oxide for Graphene Preparation. *Sci. Rep.* **2013**, *3*, 3439.
(23) Li, C.; Shi, G. Functional Gels Based on Chemically Modified Graphenes. *Adv. Mater.* **2014**, *26*, 3992−4012.
(24) Bai, H.; Li, C.; Wang, X.; Shi, G. On the Gelation of Graphene Oxide. *J. Phys. Chem. C* **2011**, *115*, 5545−5551.
(25) Ai, W.; Du, Z. Z.; Liu, J. Q.; Zhao, F.; Yi, M. D.; Xie, L. H.; Shi, N. E.; Ma, Y. W.; Qian, Y.; Fan, Q. L.; Yu, T.; Huang, W. Formation of Graphene Oxide Gel via the π-Stacked Supramolecular Self-Assembly. *RSC Adv.* **2012**, *2*, 12204−12209.
(26) Compton, Q. C.; An, Z.; Putz, K. W.; Hong, B. J.; Hauser, B. G.; Brinson, L. C.; Nguyen, S. T. Additive-Free Hydrogelation of Graphene Oxide by Ultrasonication. *Carbon* **2012**, *50*, 3399−3406.
(27) Das, A. K.; Srivastav, M.; Layek, R. K.; Uddin, M. E.; Jung, D.; Kim, N. H.; Lee, J. H. Iodide-mediated Room Temperature Reduction

of Graphene Oxide: a Rapid Chemical Route for the Synthesis of a Bifunctional Electrocatalyst. *J. Mater. Chem. A* **2014**, *2*, 1332−1340.
(28) Qi, X.; Zhou, T.; Deng, S.; Zong, G.; Yao, X.; Fu, Q. Size-specified Graphene Oxide Sheets: Ultrasonication Assisted Preparation and Characterization. *J. Mater. Sci.* **2014**, *49*, 1785−1793.
(29) Shao, G.; Lu, Y.; Wu, F.; Yang, C.; Zeng, F.; Wu, Q. Graphene Oxide: the Mechanisms of Oxidation and Exfoliation. *J. Mater. Sci.* **2012**, *47*, 4400−4409.
(30) Vanýsek, P. Electrochemical Series. *Handbook of Chemistry and Physics*, 93rd ed.; CRC Press: Boca Raton, FL, 2012; pp 5−80.
(31) Selim, R. G.; Lingane, J. J. Coulometric Titration with Higher Oxidation States of Manganese: Electrolytic Generation and Stability of +3 Manganese in Sulfuric Acid Media. *Anal. Chim. Acta* **1959**, *21*, 536−544.
(32) Cheney, M. A.; Birkner, N. R.; Ma, L.; Hartmann, T.; Bhowmik, P. K.; Hodge, V. F.; Steinberg, S. M. Synthesis and Characterization of Inorganic Double Helices of Cryptomelane Nanomaterials. *Colloids Surf., A* **2006**, *289*, 185−192.
(33) Kalra, H. L.; Ghosh, S. Kinetics and Mechanism of the Reaction Between Trivalent Manganese and Carboxylic Acids in Aqueous Solution. II. Reduction of Trivalent Manganese by Citrate. *J. Prakt. Chem.* **1965**, *30*, 6−9.
(34) Kao, W. H.; Weibel, V. J. Electrochemical Oxidation of Manganese(II) at a Platinum Electrode. *J. Appl. Electrochem.* **1992**, *22*, 21−27.
(35) Biesinger, M. C.; Payne, B. P.; Grosvenor, A. P.; Lau, L. W. M.; Gerson, A. R.; Smart, R. S. C. Resolving Surface Chemical States in Xps Analysis of First Row Transition Metals, Oxides and Hydroxides: Cr, Mn, Fe, Co and Ni. *Appl. Surf. Sci.* **2011**, *257*, 2717−2730.
(36) Nicolosi, V.; Chhowalla, M.; Kanatzidis, M. G.; Strano, M. S.; Coleman, J. N. Liquid Exfoliation of Layered Materials. *Science* **2013**, *340*, 1226419.
(37) Pupysheva, O. V.; Farajian, A. A.; Knick, C. R.; Zhamu, A.; Jang, B. Z. Modeling Direct Exfoliation of Nanoscale Graphene Platelets. *J. Phys. Chem. C* **2010**, *114*, 21083−21087.
(38) Hernandez, Y.; Nicolosi, V.; Lotya, M.; Blighe, F. M.; Sun, Z. Y.; De, S.; McGovern, I. T.; Holland, B.; Byrne, M.; Gun'Ko, Y. K.; Boland, J. J.; Niraj, P.; Duesberg, G.; Krishnamurthy, S.; Goodhue, R.; Hutchison, J.; Scardaci, V.; Ferrari, A. C.; Coleman, J. N. High-Yield Production of Graphene by Liquid-Phase Exfoliation of Graphite. *Nat. Nanotechnol.* **2008**, *3*, 563−568.
(39) Kelly, K. F.; Billups, W. E. Synthesis of Soluble Graphite and Graphene. *Acc. Chem. Res.* **2013**, *46*, 4−13.
(40) Cooper, A. J.; Wilson, N. R.; Kinloch, I. A.; Dryfe, R. A. W. Single Stage Electrochemical Exfoliation Method for the Production of Few-layer Graphene via Intercalation of Tetraalkylammonium Cations. *Carbon* **2014**, *66*, 340−350.
(41) Hu, C.; Chen, X.; Hu, S. Water-soluble Single-walled Carbon Nanotubes Films: Preparation, Characterization and Applications as Electrochemical Sensing Films. *J. Electroanal. Chem.* **2006**, *586*, 77−85.

DOI: 10.1021/acsami.5b06008
ACS Appl. Mater. Interfaces 2015, 7, 21356−21363